

Strong Ground Motion Synthesis for a M=7.2 Earthquake in the Gulf of Corinth, Greece Using Empirical Green's Functions

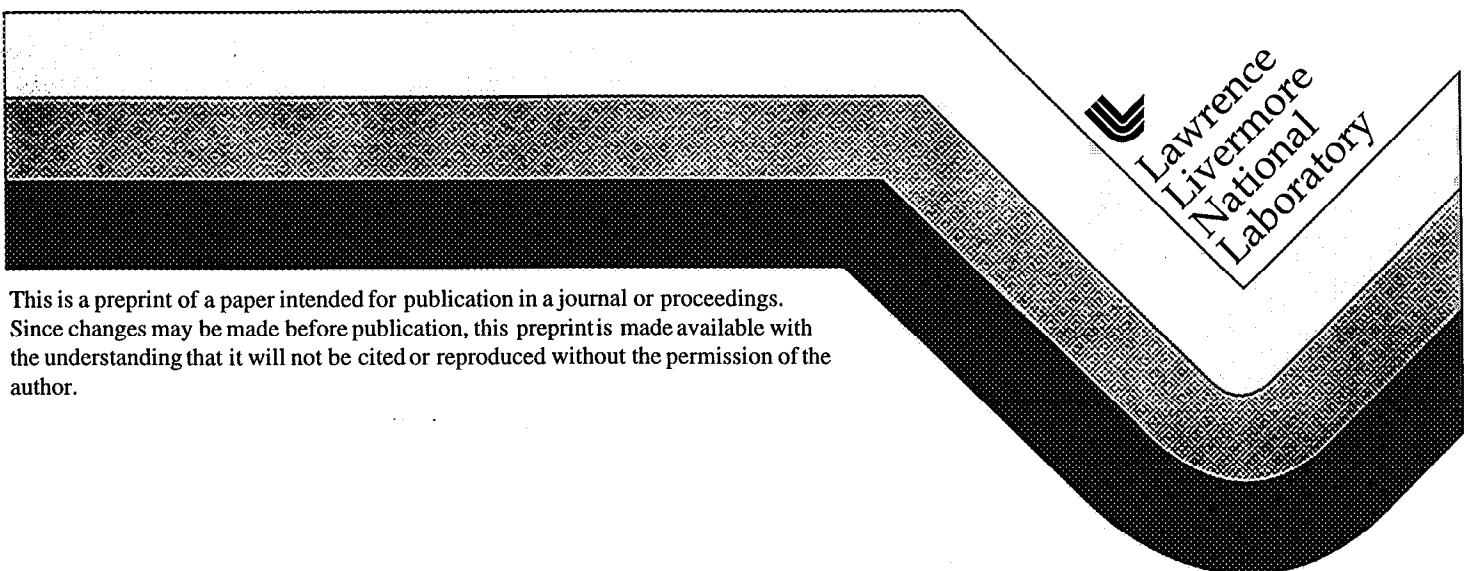
Lawrence Hutchings (1) Giorgis N. Stavrakakis (2) Eleni Ioannidou (3) Francis T. Wu
(4) Steve Jarpe (5) Paul Kasameyer (1)

- (1) Lawrence Livermore National Laboratory, Livermore, CA
(2) Geophysic and Geothermy Division University of Athens, Athens, Greece
(3) Ministry of Education, 1st T.E. L. of Chalkida, Chalkida, Greece
(4) Department of Geological Sciences, State University of New York, Binghamton, NY
(5) Institute for Crustal Studies, University of California, Santa Barbara, CA

This paper was prepared for submittal to the

29th IASPEI General Assembly
Thessaloniki, Greece
August 18–28, 1997

January 1998



This is a preprint of a paper intended for publication in a journal or proceedings. Since changes may be made before publication, this preprint is made available with the understanding that it will not be cited or reproduced without the permission of the author.

DISCLAIMER

This document was prepared as an account of work sponsored by an agency of the United States Government. Neither the United States Government nor the University of California nor any of their employees, makes any warranty, express or implied, or assumes any legal liability or responsibility for the accuracy, completeness, or usefulness of any information, apparatus, product, or process disclosed, or represents that its use would not infringe privately owned rights. Reference herein to any specific commercial product, process, or service by trade name, trademark, manufacturer, or otherwise, does not necessarily constitute or imply its endorsement, recommendation, or favoring by the United States Government or the University of California. The views and opinions of authors expressed herein do not necessarily state or reflect those of the United States Government or the University of California, and shall not be used for advertising or product endorsement purposes.

Strong Ground Motion Synthesis for a M=7.2 earthquake in the Gulf of Corinth, Greece using Empirical Green's functions

*presented, 29th IASPEI General Assembly
Thessaloniki, Greece, August 18-28, 1997*

Lawrence Hutchings¹; Giorgis N. Stavrakakis²; Eleni Ioannidou³; Francis T. Wu⁴; Steve Jarpe⁵; Paul Kasameyer¹

1) Lawrence Livermore National Laboratory, P.O. Box 808, Livermore Ca. 94551, USA; telephone (510) 423-0354, fax: (510) 422-3925, email: hutchings2@llnl.gov

2) Geophysic and Geothermy Division, University of Athens, P.O. Box 20048, 118 10 Athens, Greece; email: g.stavr@ege.lados.gein.noa.gr

3) Ministry of Education, 1st T.E.L. of Chalkida, Chalkida 34100 Greece; telephone 30-221-292, e-mail: elioan@acropolis.net

4) Department of Geological Sciences, State University of New York, Binghamton, New York, 13902-6000, USA; telephone: (607)777-2512; fax: (607)777-2288; email: wu@sunquakes.geol.binghamton.edu

5) Institute for Crustal Studies, University of California, Santa Barbara, California 93106-9630, USA; telephone: (520) 775-6803; email: jarpe@computerlink.com.

Abstract

We synthesize strong ground motion at three sites from a M=7.2 earthquake along the NW-trending Gulf of Corinth seismic zone. We model rupture along an 80 segment of the zone. The entire length of the fault, if activated at one time, can lead to an event comparable to that of the 1995 Kobe earthquake. With the improved digital data now routinely available, it becomes possible to use recordings of small earthquakes as empirical Green's functions to synthesize potential ground motion for future large earthquakes. We developed a suite of 100 rupture scenarios for the earthquake and computed the commensurate strong ground motion time histories. We synthesized strong ground motion with physics-based solutions of earthquake rupture and applied physical bounds on rupture parameters. The synthesized ground motions obtained are source and site specific. By having a suite of rupture scenarios of hazardous earthquakes for a fixed magnitude and identifying the hazard to a site from the statistical distribution of engineering parameters, we have introduced a probabilistic component to the deterministic hazard calculation. The time histories suggested for engineering design are the ones that most closely match either the average or one standard deviation absolute acceleration response values.

Introduction

Realistic time histories should be used to reduce uncertainties in estimation of standard engineering parameters (Hutchings, 1991) and for nonlinear dynamic analysis of structures (McCallen and Hutchings, 1996). Here we present a methodology for developing realistic synthetic strong ground motions for specific

sites from specific faults. We hypothesized a M=7.2 earthquake (moment magnitude, Hanks and Kanamori, 1979) that ruptures 80 km along the Gulf of Corinth seismic zone (Figure 1) as an example of a design earthquake calculation. The length of the fault, if activated at one time, can lead to an event comparable to that of the 1995 Kobe earthquake. We synthesize strong ground motion at three sites: 2, 8,

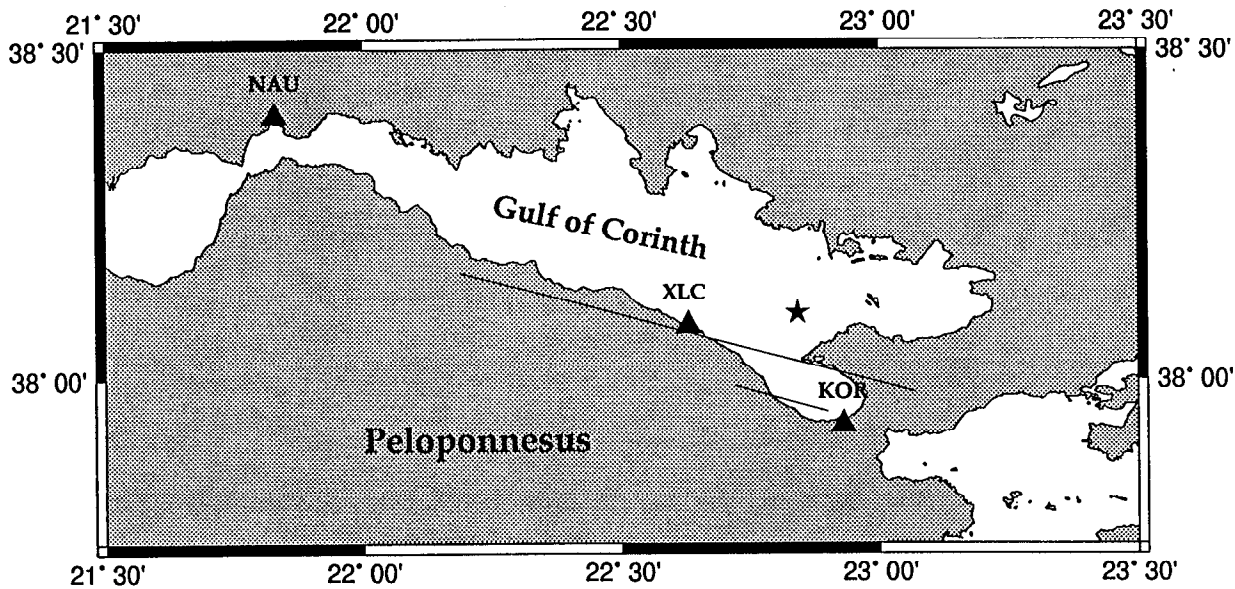


Figure 1. Map showing the area of Greece that is being studied. The triangles show the three station locations, XLC and NAU, and KOR. The star is the epicenter of the Ms=6.7 24 February 1981, Corinth, central Greece earthquake, the short line segment is the surface intersection of the rupture plane of that earthquake, and the longer line segment is the surface intersection of the rupture plane of the hypothesized M7.2 earthquake.

and 48 km from the hypothesized fault (Table 1 and Figure 1).

Realistic time histories should include the effects of geologic conditions along the propagation path from the fault and at the site itself. Geologic conditions can significantly alter the amplitudes of seismic energy, and can cause focusing and scattering of energy. Also, at sites close to large faults it is critical to account for the effects of finite fault rupture. These include seismic arrivals radiated from portions of the fault that can be tens of kilometers apart and arrive at the same time, and directivity effects that can significantly enhance or diminish amplitudes of the wave field. In addition, the superposition of direct and scattered body-waves and surface-waves will result in an extremely complicated wavefield and should be modeled. To model all these affects we synthesize strong ground motion with physics

based solutions of earthquake rupture that utilize empirical Green's functions and apply physically based rupture parameters. We have developed an exact solution to the representation relation for finite rupture that utilizes either empirical or synthetic Green's functions (Hutchings and Wu, 1990; Hutchings, 1991; Jarpe and Kasameyer, 1996). Here, we use recordings of small earthquakes to provide empirical Green's functions for frequencies 0.5 to 5.0 Hz, and analytical calculations to provide synthetic Green's functions for frequencies 0.05 to 0.5 Hz. We synthesize the entire wavetrain and for three components. Site soil can also significantly affect ground motions with non-linear effects, but here we only present linear ground motions that might be expected at a rock outcrop.

Table 1: Strong Motion Sites

Site	Latitude	Longitude	Distance
XLC	38.08	22.63	2 km
NAU	38.40	21.83	48
KOR	37.93	22.93	8

Gulf of Corinth

The Gulf of Corinth (Figure 1) occupies a zone of crustal extension which is an integral part of the Aegean Orogene and has long been recognized as a graben structure (or rift valley) formed by normal faulting (Tselentis and Makropoulos, 1986). It is approximately 150 km long and 20 km wide. Tselentis and Makropoulos (1986) studied the deformation in the gulf. Their interpretation is that the variation in stress directions indicates that two different tectonic processes control the evolution of the Corinth rift. The first involves westward obduction of the Peloponnesos with a clockwise rotation, which explains the eastward widening of the Gulf. The second process is related to crustal arching along an axis trending roughly E-W. Vertical movement is restricted mainly to a relatively narrow crustal zone and has resulted in northward and southward tilting (Tselentis and Makropoulos, 1986).

The Gulf of Corinth has long been known as a region of pronounced seismicity, with expected maximum earthquake magnitude $M_s = 7.2$ (Drakopoulos and Makropoulos, 1983). Several historical events occurred along the Gulf of Corinth seismic zone; 26 earthquakes with $M \geq 5.0$ have occurred since 1902. The

$M_s=6.3$, 1928 Corinth earthquake caused considerable damage in and around the town of Corinth (Drakopoulos *et al.*, 1978). The $M_s=6.7$ 24 February 1981, Corinth, central Greece earthquake; two $M_s=6.4$ aftershocks, on 25 February and 4 March are the largest recent earthquakes to occur in the seismic zone; and significant surface faulting and geomorphical changes have been observed (Vita-Finzi and King, 1985; Jackson *et al.*, 1982; Stavrakakis, 1982). Tselentis and Makropoulos (1986) evaluated focal mechanism solutions from all available historical earthquakes and concluded that the principle stress is north-south extension. Ioannidou (1989) recalculated moment tensor solutions for all moderate and large greek earthquakes for the years 1965-1988 and found that the principle stress orientation in the gulf Corinth to be north-south extension.

Source Models

The synthesis approach uses empirical Green's functions solely to obtain the Green's functions of the representation relation, thereby allowing for completely synthetic rupture models (Wu, 1978; Hutchings and Wu, 1990). Thus, *no a priori* assumptions are imposed on the rupture process, and a suite of kinematic rupture models can be used.

Several observations indicate that many earthquakes are in fact complex or multiple events (Wyss and Brune, 1967; Wu and Kanamori, 1975; Fuko and Furumoto, 1975). Complex events have also been proposed in the numerical modeling of faulting with variable strength by Das and Aki, 1977; Mikumo and Miyatake, 1978. We model the 24 February 1981, $M=6.7$ Corinth, central Greece, earthquake with a complex rupture model developed by Stavrakakis *et al.* (1982) and Jackson *et al.* (1982). We use results from this calibration

study to provide constraints on modeling the larger $M=7.2$ hypothesized earthquake.

We model the rupture process as a continuous rupture over fault segments with variable slip amplitude. Areas of high slip are called asperities. Typically, we include one to several asperities for a rupture model. This asperity model is consistent, within the frequency range of resolution, with inversion studies that show few to several area of high slip amplitude (Wald et. al., 1990, 1991, 1993, 1995; Beroza and Spudich, 1988; Hartzell and Heaton, 1988; Hartzell 1989) and with what is known from dynamic rupture models about how earthquakes rupture (Rice and Ruina, 1983; Kostrov and Das, 1988). However, these studies only resolve fault slip histories up to spatial resolutions of a couple of kilometers and frequencies up to one hertz. Nevertheless, our method provides good fits to observed seismograms up to 25 Hz when these models are used.

Most empirical Green's functions synthesis approaches model fault rupture as a composite of smaller earthquakes, which have a multitude of small events rupturing independently over the fault surface (Hartzell, 1978; Hadley and Helmberger, 1980; Irikura, 1983; Papageorgiou and Aki, 1983; Munguia and Brune, 1984; Joyner and Boore, 1986; Boatwright, 1988; Wennerberg, 1990; and, Aki and Irikura, 1991). There is little physical or empirical basis for composite models of earthquakes with this degree of complexity. Also, composite models of faulting rely on scaling relations of earthquakes to determine the number of small earthquakes necessary to synthesize a large earthquake, and have a difficulty in matching the low and high frequency of synthesized seismograms to observed records (Joyner and Boore, 1986; Boatwright, 1988; Tumarkin *et. al.*, 1994; Frankel 1995). Our modeling approach only requires that the number of small

earthquakes used in the synthesis is such that the sum of their moments add up to the moment of the large earthquake, which matches the low frequency of observed seismograms. The high frequency is matched simply by using appropriate rupture parameters (Hutchings, 1994).

We developed a suite of 100 rupture scenarios for the hypothesized $M=7.2$ earthquake on the Gulf of Corinth fault zone and computed the commensurate strong ground motion time histories. The scenarios were developed by randomly varying rupture parameters within a range of physical limits obtained from independent research. This approach is useful if the range of possible fault rupture histories is narrow enough to functionally constrain the range of strong ground-motion predictions. Log-normal average and one standard deviation values of peak acceleration, pseudo-velocity response, and absolute acceleration response spectra were derived from the suite of synthesized strong ground motion. By having a suite of rupture scenarios of hazardous earthquakes for a fixed magnitude and identifying the hazard to the site from the one standard deviation value of engineering parameters, we have introduced a probabilistic component to the deterministic hazard calculations.

Green's Functions

The basic premise in synthesizing with empirical and synthetic Green's function is that each offers the best accuracy over particular frequency bands. Empirical Green's functions are defined here as recordings of effectively impulsive point source events (Hutchings and Wu, 1990). The empirical Green's functions have a better accuracy at high frequencies, where geologic inhomogeneities are not well modeled, and the synthetic Green's functions

have better accuracy at lower frequencies, where empirical Green's functions do not have sufficient energy. The overlap in this study is in the range from $3 \leq f \leq 5$ Hz, where the geology can be modeled with some accuracy and the empirical Green's function have sufficient energy to be well recorded.

We computed synthetic Green's functions using the reflectivity code of Kennett (1983). This solution extends to D.C., but does not include near-field terms. Focal mechanism radiation pattern is used for synthetic Green's functions solutions to the finite rupture. We only considered solutions for frequencies greater than 0.05 Hz (20 sec period), as lack of near-field arrivals diminish the reliability of solutions for frequencies lower than this. A one dimensional velocity model was used for the calculations.

Empirical Green's functions should be recorded at the site of interest and from source events along the faults of interest, since site response and near source propagation path effects are highly variable. Empirical Green's functions include the actual effects of velocity structure, attenuation, and geometrical spreading. However, it is not possible to record empirical Green's functions from all locations along a fault of interest and with the same focal mechanism solution, so that source locations of empirical Green's functions have also been interpolated to fill in the fault. Figure 1 shows epicenter locations of source events used for empirical Green's functions. The limited locations of events that provide empirical Green's functions means that the site response is primarily captured by the empirical Green's functions, and that propagation path effects from locations to the south of the site area are not captured. The spatial dependence of empirical Green's functions has been

researched by Hutchings and Wu (1990) and they found that the variability in ground motion due to differences in source location and/or focal mechanism solutions are much less than that due to the site response, and Hutchings (1991), Hutchings (1994), and Jarpe and Kasameyer (1996) found that interpolation for different source locations along a fault works quite well. Also, it is not necessary to have source events fall directly along the fault of interest, but to be located near the fault. In synthesis, we have the option of correcting for different focal mechanism solutions, but Hutchings and Wu (1990) and Jarpe and Kasameyer (1996) found that for high frequencies it does not improve the synthesis. Interpolation is performed by correcting for attenuation, $1/R$, and P- and S-wave arrival times due to differences in source distance. We include the radiation pattern effect for low frequencies, when we use synthetic Green's functions. The use for empirical Green's functions at each site (Kalogeras and Stavrakakis, 1996):

events (NAU)	location			moment
event1	38.43	21.75	9.0	0.794E+22
event2	38.16	21.76	9.0	0.891E+23
event3	38.34	21.85	9.0	0.100E+22
event4	38.37	21.94	9.0	0.316E+23

events (XLC)	location			moment
event1	38.14	22.56	9.0	0.562E+23
event3	38.16	22.62	9.0	0.316E+24

events (KOR)	location			moment
event1	38.10	22.85	9.0	0.100E+22
event4	37.91	23.15	9.0	0.316E+24

Corinth Earthquake Synthesis

A forward model of the Corinth earthquake is calculated to test hypotheses about rupture models, validate the methodology used in this study, and to calibrate aftershock source

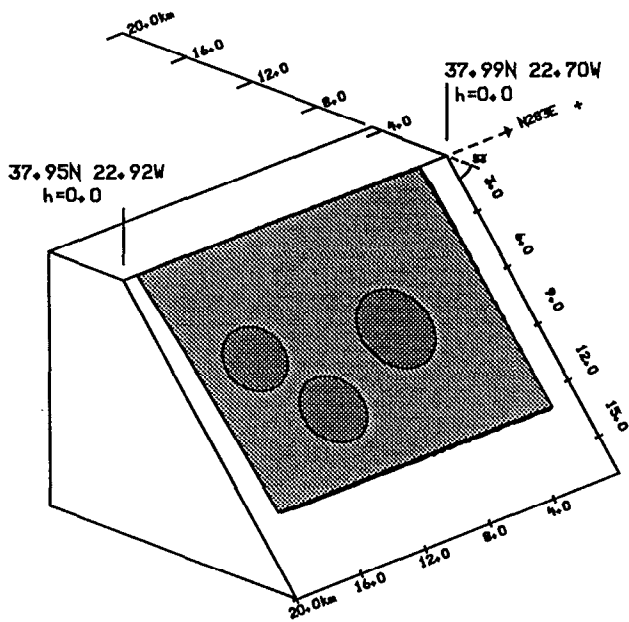


Figure 2. Source rupture model for the $M=6.7$, 1981 Corinth earthquake. Circle are hypothesized asperity locations.

parameters. Stavrakakis et al. (1982) utilized long period P-waves recorded by WWSSN stations in an iterative deconvolution to a model for source complexity. This model is used here to synthesize observed strong motion records at site XLC (Figure 1, Table 1).

Observed surface faulting and the relocated hypocenter (Jackson et al. (1982) is used to constrain the source geometry for this earthquake. Figure 1 shows modeled surface faulting from this study. The hypocenter is 38.099N 22.842W $h=10.0$ (star in Figure 1) from Jackson et al. (1982); the moment is 7.19×10^{25} dyne-cm, the focal mechanism solution is strike $N283^\circ E$, dip 44° , and slip vector rake -72° , faulting duration is 9 seconds, and fault dimensions are 15 km long by 15 km wide from Jackson et al. (1982). Figure 2 shows a

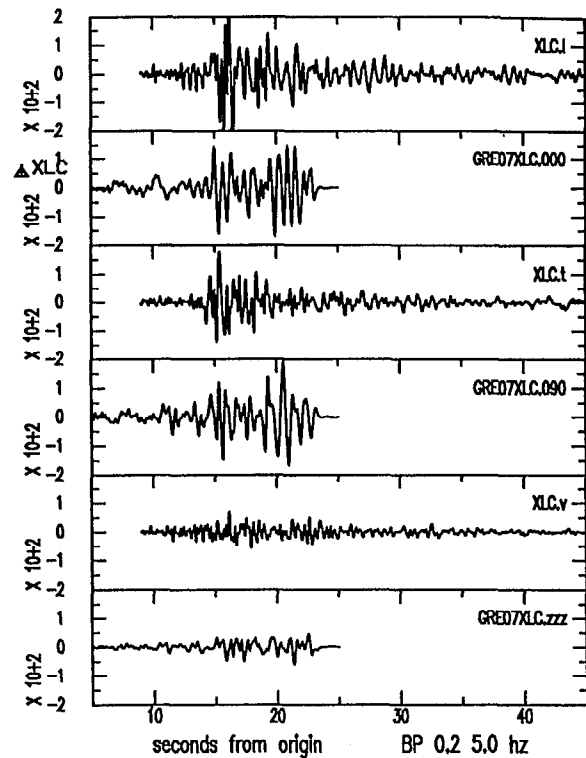


Figure 3. Observed (top) and synthesized accelerograms (bottom) for three components.

fault rupture model that has an asperity distribution similar to three principle asperities identified by Stavrakakis et al. (1982). Accelerograms compared to observed records. The asperities are at greater depth than proposed by Stavrakakis et al. (1982) and the dip is shallower, but considering the uncertainty in their study this model probably fits. A rupture velocity $0.75V_s$ was used. Figure 3 shows observed and synthesized accelerograms. It is evident that this model captures the amplitude, frequency content and energy distribution of the actual records. This model provided the best fit accelerograms. Records are band passed from 0.2 to 5.0 Hz. The frequency is limited by the frequency range of the empirical Green's functions.

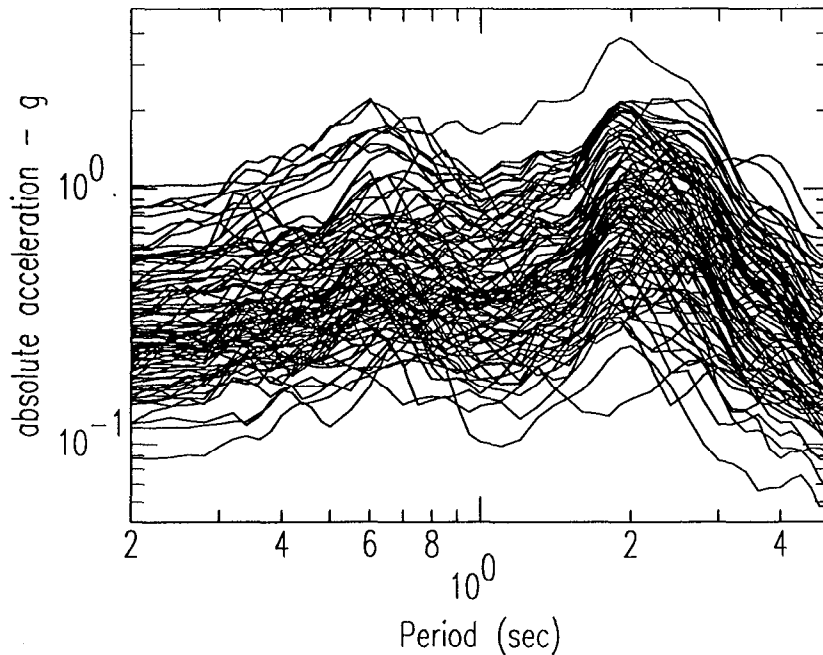


Figure 3. The AAR response curves for the 100 scenarios.

Gulf of Corinth Seismic Model

The NW-SE-trending seismic zone in the shallow crust of the Gulf of Corinth is modeled here as capable of a magnitude 7.2 earthquake ($M_0 = 7.01 \times 10^{26}$ dyne-cm). Vita-Finzi and King (1982) and Jackson et al. (1982) propose that the current active portions of the seismic zone lie primarily north of the city of Corinth (Figure 1). Surface faulting from recent earthquakes is observed in this area and this is supported by historical and archaeological data (Vita-Finzi and King (1982)).

Vita-Finzi and King interpret surface faulting and morphological features to hypothesize the existence of faults at depth (see their figure 7). A continuous feature that extends the length of the Gulf of Corinth and runs through the area where surface faulting was observed from the 1981 events is selected as the surface expression of the fault to be modeled in this study.

We model rupture along an 80 km segment (although this varies by ± 10 km for multiple runs).

Moment of aftershocks used as empirical Green's functions were determined from body-wave magnitudes reported by Kalogeras and Stavrakakis (1996) and the moment magnitude relation of $\log M_0 = 1.5M_b + 15$. The moment magnitude relation was modified from Hanks and Kanamori (1979) by matching observed and synthesized records of the $M=6.7$ Corinth earthquake.

Synthetic Rupture Models

Our earthquake rupture models rely on moment, fault geometry, hypocenter, rupture roughness, rupture velocity, healing velocity, slip vector, and asperity location. Moment and fault geometry (extent of rupture and its orientation) are held fixed, while the other parameters were allowed to vary within limits. The fault rupture

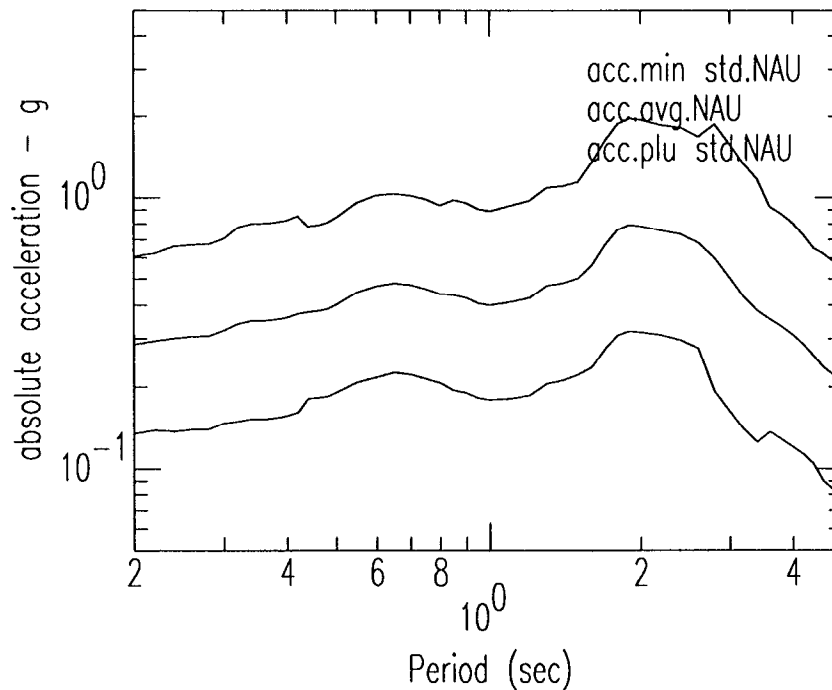


Figure 4. Mean and one standard deviation values of AAR.

surface area was discretized into 0.01 Km^2 elemental areas, which are small enough that modeled rupture is continuous for frequencies $f \leq 25.0 \text{ Hz}$. The rupture initiates at the hypocenter and propagates radially at some fraction of the shear wave velocity. We used the Kostrov slip function to calculate the slip at a point; we approximated the shape as a ramp. We arbitrarily limited the rupture propagation factor in the Kostrov slip function to be equal to or less than the rupture time to the closest fault edge from the hypocenter. We used a computer program that randomly varies independent rupture parameters subject to the following constraints. Other parameters are either fixed or calculated from the rupture model.:

ASPERITIES are included to add high slip amplitudes to portions of the rupture. Asperities are circular and have a diameter randomly cho-

sen to be between 0.2 and 0.8 times the fault width. The number of asperities is randomly selected for each scenario. Stress drop in asperity portions of rupture are higher than elsewhere.

ROUGHNESS is simulated as elements resisting rupture, then breaking. A percentage of elements (0, 10, 20, 33, or 50%) have a shortened rise times 10-90% those of neighboring elements, but with rupture completed at the same time as neighboring elements. These "rough" elements have corresponding high stress drop.

MOMENT is constrained to be 7.0×10^{26} dyne-cm for the total rupture, including asperities. However, the moment of asperities is randomly selected, subject to the constraint that the maximum displacement is 5-10m.

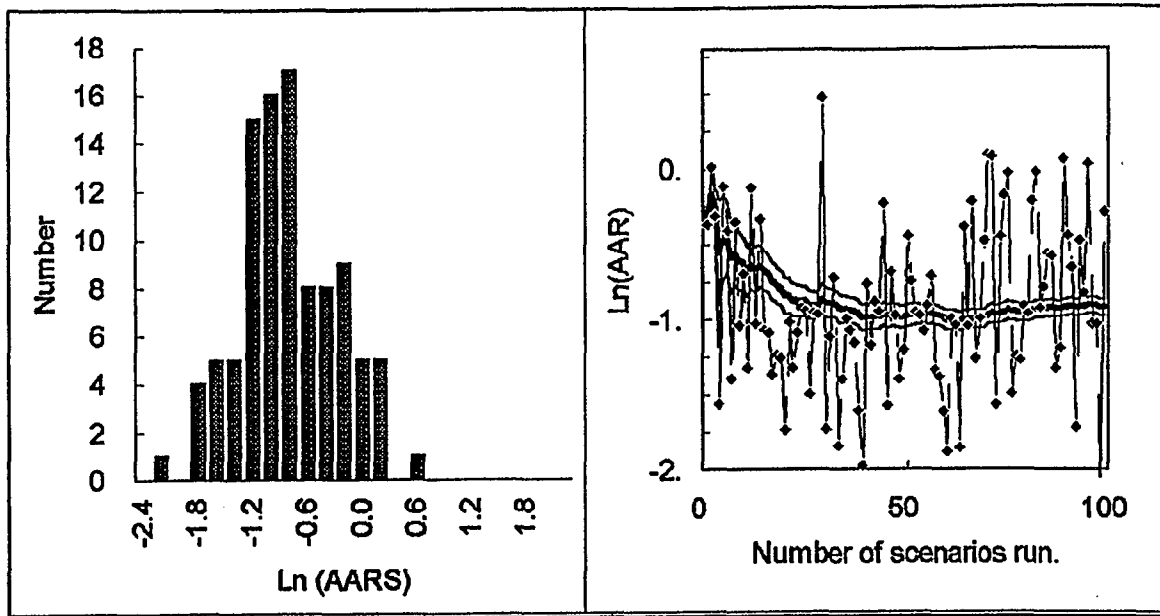


Figure 5. Histograms of number of scenarios as a function of AAR at 1.0 second period

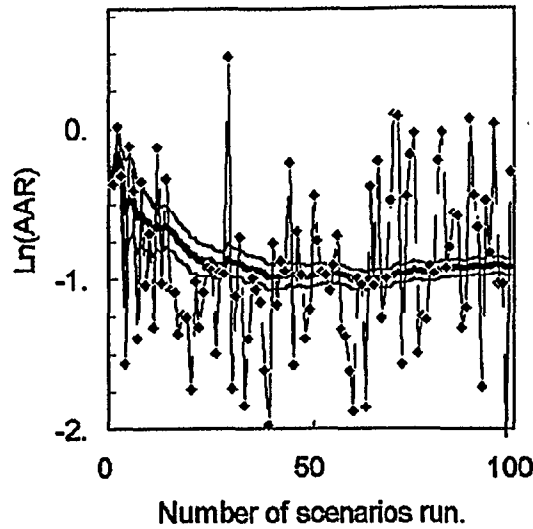


Figure 6. Estimation of the mean (dark line) AAR at 1.0 s, its uncertainty, and the individual AAR values.

Rigidity (proportional to shear wave velocity, except near the surface) diminishes near the surface so that the moment contribution diminishes. However, stress drop is also modeled to diminish (discussed below), so significant displacement can occur near the surface, although not seismogenic.

HYPOCENTER was constrained to occur at least 1 km from the fault ends, 2 km from the lower limit of the fault, and at depth greater than 7.5km. The limit at the lower portion of the fault is because of the weakening in rigidity as the aseismic zone is approached, and the limit to greater than 7.5 km is due to the observation that past earthquakes originate at depth.

RUPTURE VELOCITY is randomly selected to be from 0.75 to 1.0 times the shear wave velocity.

HEALING VELOCITY is the velocity for the stress pulse that terminates slip. The healing phase is initiated after the rupture arrives at any fault edge. The free surface is not allowed to be

a healing boundary for rupture, because significant seismic pulses that are necessary to shut down slip are not generated from the surface (Das and Kostrov, 1985; Scholz, 1990). The healing velocity is randomly selected to be between 0.8 and 1.2 times the rupture velocity, which is between the Rayleigh and shear wave velocities.

RISE TIME is equal to the time it takes, after the initiation of rupture, for the first healing phase to arrive.

STRESS DROP is a dependent variable derived from the Kostrov slip function and allowed to vary due to three effects modeled in rupture. Asperities and rough rupture are allowed to have a different stress drop than surrounding portions of the fault rupture (discussed above). Also, stress drop is constrained to diminish near the surface of the earth at the rate of $10 + 0.75 \times$ the confining pressure due to the lithostatic load (300 bars at 1.7 km depth). The minimum of the stress drop calculated using this constraint and

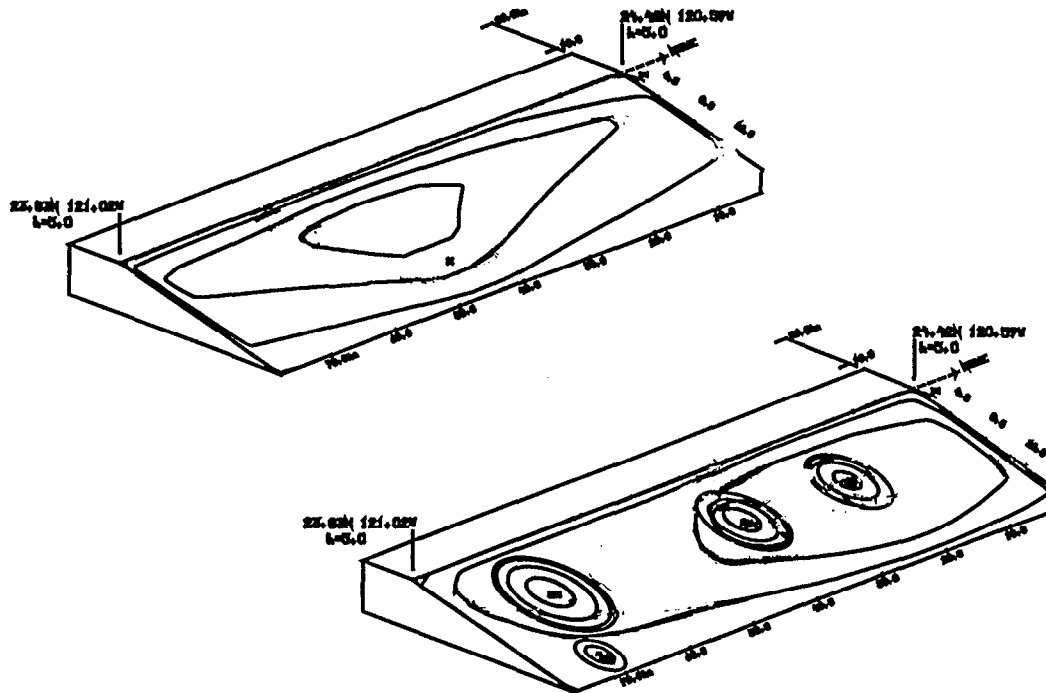


Figure 7. Slip distribution and fault geometry for models TAI01 (top) and TAI33 (bottom). The location of the hypocenter is shown by the asterisk, and the location of the site (TCU128) is shown by the triangle.

the full rupture stress drop is used.

SLIP VECTOR is constrained to 135° for equal portions of reverse and right-lateral strike slip fault motion.

Prediction Uncertainty

In the terminology of Abrahamson et al., 1990), our prediction uncertainty has two elements: 1) parametric uncertainty, which arises from uncertainty as to which scenario will occur, and (2) modeling and random errors caused by not modeling the actual rupture process correctly and by factors such as uncertainties in moment estimates for empirical Green's functions and errors caused by interpolation of source events along the fault surface.

We estimated the parametric uncertainty by generating a suite of time histories from 100 sets of independent parameters. We selected these sets at random by assuming that the parameters are uncorrelated and that each is uniformly distributed through its allowed range. Figure 3 shows the average (in log space) of the absolute acceleration response (AAR) spectra for the two horizontal components calculated for each of the 100 parameter sets. All these parameter sets represent earthquakes with the same moment and fault rupture area, parameters that might be successfully anticipated in advance. As Figure 3 shows, a broad range of possible response spectra could be generated from an event whose moment and fault rupture area are fixed.

Jarpe and Kasameyer (1996) estimated the second element of uncertainty, modeling and random errors, by comparing computed and observed records for the 1989 Loma Prieta earthquake, whose independent parameters were well determined. This error is unknown for the site at NSY, but is assumed to be equal to the one standard deviation value obtained by Jarpe and Kasameyer (1996). The total source uncertainty is characterized by adding the parametric and “random plus modeling” standard deviation estimates (0.80 and 0.55 at 1 Hz) in quadrature. The mean and 84th percentiles of the AAR distribution calculated in this manner are given by the dark line in Figure 4. The average peak acceleration is 0.29g, and the plus one standard deviation value is 0.49g.

We examine the AAR data at a single frequency (1Hz) to illustrate how the parametric error can be estimated and how that estimate is improved by calculating more scenarios. Figure 5 is a histogram of the natural logarithms of the calculated values at that frequency. The data are distributed normally in log-space with a sample mean and standard deviation of -2.85 and 0.53, and they pass a χ^2 test (Freund, 1962) for the log normal distribution. Figure 6 shows the evolution of the sample mean as a function of the number of scenarios run. The uncertainty in the mean is estimated from the observed variability and number of points used, approximating the data-distribution as log-normal. A similar calculation was made for the “84th percentile” represented by the sum of the sample mean and sample standard deviation. The uncertainty in the sum is estimated by assuming the errors in the mean and standard deviation are independent (Hald, 1952). Estimates of the mean and 84th percen-

tile vary significantly with the number of scenarios, but the final estimates (for 100 scenarios) always lie within the 1σ bounds for the estimate uncertainty, suggesting that the approximate error model gives a useful estimate of the uncertainty. The uncertainties decrease significantly as more scenarios are added. The uncertainty in the natural logarithm of the mean decreased from 0.14 after 10 scenarios, to 0.05 (corresponding to approximately 0.003g) after 100. The bounds for the 84th percentile are about $\pm 0.01g$ after 100 runs

Hazard

A methodology for identifying the ground motion hazard to a site is to choose an acceptable probability from the suite of hazards from the 100 scenarios. If either the mean or $+1\sigma$ AAR (50th or 84th percentile) is chosen to identify the hazard, then time histories with AAR near these values would represent the hazard. It is not recommended to modify AAR to match a “target” spectrum, because this would effectively alter the rupture scenario and may inadvertently generate a non-physical model. Further, in non-linear structural analysis more than one time history should be selected. Rupture models GRE01 and GRE33 generated time histories that had AAR closest to the mean and $+1\sigma$, respectively. Figure 7 shows the slip distribution and hypocenter for these models. Figure 8 shows the time histories; the top three are the three components of acceleration, the middle three are the same records integrated to displacement, and the bottom three are the displacement values.

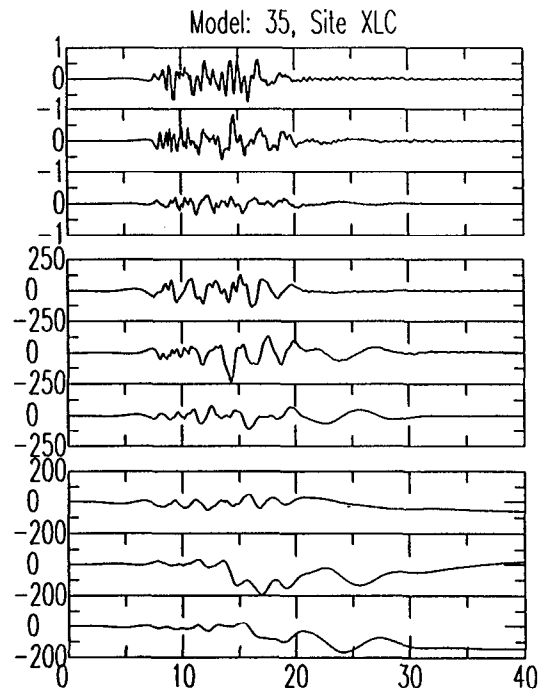
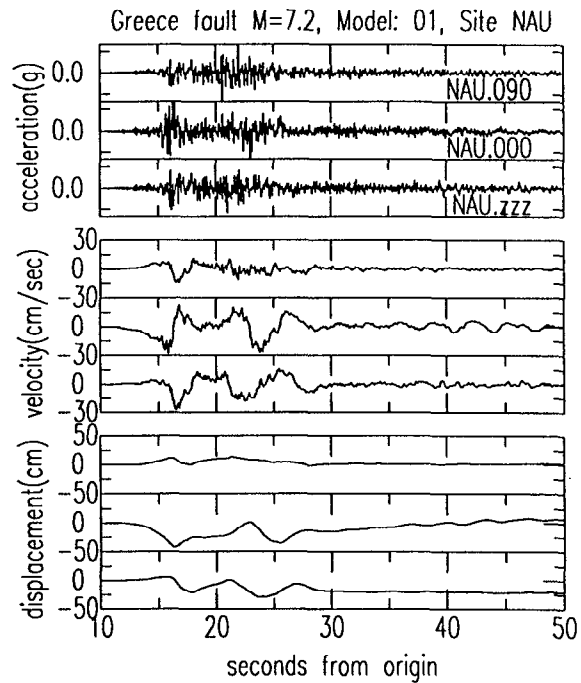
Discussion

The hazard for a possible M=7.2 earthquake along the Gulf of Corinth seismic zone was

predicted at three sites. The work presented here is a demonstration of a methodology to predict a range of ground motion hazard. This allows for a probabilistic component in selecting the hazard for engineering design purposes. From Figure 8, the model that most closely matches the mean hazard shows peak accelerations near 0.3g and durations greater than 10 seconds. Figure 7 shows that this ground motion is due to a fairly smooth rupture model that does not include asperities. The same model that most has peak accelerations near 1.0g at XLC and durations that are similar to those of site NAU.

The methodology presented provides a means to model all the physical effects of finite fault rupture. The velocity records show a long period “fling” due to fault-normal directivity effects. Since station XLC is located directly above a portion of the fault, one would also expect a static offset left after the earthquake. This is evident in Figure 8 displacement plots.

Empirical Green’s functions provided a means to constrain the uncertainties due to geologic inhomogeneities. However, the sensitivity of the instrumentation was such that only fairly large earthquakes ($M > 3.0$) located nearby were recorded, and could provide empirical Green’s functions. To improve constraints on geological effects at greater distances, lower gain settings would have to be applied. Also, the instrumentation noise level was such that frequencies below about 5.0 Hz were not well recorded. This necessitated using synthetic Green’s functions for frequencies higher than their expected reliability.



References

- Abrahamson, N. A., P. G. Somerville, and C. A. Cornell (1990), *Uncertainty in Numerical Strong Motion Predictions*, in *Proc. 4th U.S. National Conf. Earthquake Engineering*, Vol. 1 (Earthquake Engineering Research Institute, 20–24 May, Palm Springs, California).
- Aki, K., and K. Irikura (1991). Characterization and mapping of earthquake shaking for seismic zonation, in *Proceedings of the Fourth International Conference on Seismic Zonation, Vol. I*, EERI, Oakland, 61-110.
- Beroza, G.C. and P. Spudich (1988) Linearized inversion for fault rupture behavior: application to the 1984 Morgan Hill, California earthquake. *J. Geophys. Res.* **93** 6275-6296.
- Boatwright, J. (1988). The seismic radiation from composite models of faulting, *Bul. Seis. Soc. Am.* **78**, 489–508.
- Das, S., and B. V. Kostrov (1985), *An Elliptical Asperity in Shear: Fracture Process and Seismic Radiation*, *Geophys. J. Roy. Astron. Soc.* **80**, 725–742.
- Drakopoulos, J.K. and K.C. Makropoulos (1983) Seismicity and hazard analysis studies in the area of Greece. Univ. of Athens, Seismol. Lab., Publ. 2: 126 pp.
- Drakopoulos, J., G. Leventakis and A. Roussopoulos (1978). Microzonation in the seismic area of Corinth-Loutraki, *Ann. Geofis.* **31**, 51-96.
- Foxall, William, Lawrence Hutchings, and Paul Kasameyer (1995) Lithological and Rheological Constraints on Fault Rupture Scenarios for Ground Motion Hazard Prediction. *IUTM Symposium on Mechanics Problems in Geodynamics*, Sept. 5-9, 1994, Beijing, China; UCRL-JC 116437 Lawrence Livermore National Laboratory, pp 27. submitted to *Bul. Seis. Soc. Am.*
- Foxall, William (1992) Heterogeneous Slip and Rupture Models of the San Andreas Fault Zone based upon Three-Dimensional Earthquake Tomography. dissertation, University of California, Berkeley, pp.168.
- Frankel, Arthur (1995) Simulating strong motion of large earthquakes using recordings of small earthquakes: the Loma Prieta main shock as a test case. *Bul. Seis. Soc. Am.* **85**, pp. 1144-1160.
- Freund, John E., *Mathematical Statistics*, 390 pp., Prentice-Hall, Englewood Cliffs, NJ., 1962.
- Hadley, D.M. and D.V. Helmberger (1980). Simulation of strong ground motions. *Bul. Seis. Soc. Am.* **70**, 617-630. Hald, A., *Statistical Theory with Engineering Applications*, John Wiley and Sons, New York, 1952 (1952).
- Hanks, T.C. and H. Kanamori (1979) A moment magnitude scale. *J. Geophys. Res.* **84**, 2348–2350.
- Hartzell, S. (1989) Comparison of seismic waveform inversion results for the rupture history of a finite fault: application to the 1986 North Palm Springs, California earthquake. *J. Geophys. Res.* **94** 7515-7534.
- Hartzell, S.H. (1978). Earthquake aftershocks as Green's functions, *Geophys. Res. Lett.* **5** (1)
- Hartzell, S.H. and T.H. Heaton (1988) Inversion of strong ground motion and teleseismic waveform data for the fault rupture history of the 1979 Imperial Valley, California, earthquake. *Bul. Seis. Soc. Am.* **73**, pp. 1533-1583.
- Heaton, T. H. (1982). The 1971 San Fernando earthquake: a double event? *Bul. Seis. Soc. Am.* **72**, 2037–2062.
- Hsu, C.-H., C.-I Lee, and J.-F. Lee (1996) NW-SE trending seismic zone in the Miaoli-Taichung-Nantou area, central Taiwan, and its implication in tectonics, in *Proceedings of the joint symposium on Taiwan Quaternary [6] and on investigation of subsurface geology and engineering environment of Taipei basin*, 224-228.
- Hutchings, L. (1988). Modeling strong earthquake ground motion with an earthquake simulation program EMPSYN that utilizes empirical Green's functions, Lawrence Livermore National Laboratory, Livermore, CA, *UCRL-ID-105890*, p. 122.
- Hutchings, L. (1991). "Prediction" of strong ground motion for the 1989 Loma Prieta earthquake using empirical Green's functions, *Bul. Seis. Soc. Am.* **81**, 88–121.
- Hutchings, L. (1994) Kinematic Earthquake Models and Synthesized Ground Motion Using Empirical Green's Functions. *Bul. Seis. Soc. Am.* **84**, pp. 1028-1050.
- Hutchings, L. and F. Wu (1990). Empirical Green's functions from small earthquakes—A waveform study of locally re-

- corded aftershocks of the San Fernando earthquake, *J. Geophys. Res.* **95**, 1187–1214.
- Hutchings, L. and S. Jarpe (1996) Ground motion Variability at the Highways 14 and I-5 Interchange in the Northern San Fernando Valley. *Bul Seis Soc Am.* **86**, S289-S299.
- Ioannidou, Eleni (1989) Seismic source parameters from inversion of teleseismic bodywaves: A study of all moderate and large greek earthquakes for the years 1965-1988. Ph.D. Thesis University of Athens, 1989.
- Irikura, K. (1983). Semi-empirical estimation of strong ground motions during large earthquakes. *Bull. Disaster Res. Inst.*, Kyoto Univ., **33**, 63-104.
- Jackson, J. A., Gagnepain, J., Houseman, G., King, G.C.P., Papadimitriou, P., Soufleris, C. & Virieux, J. (1982) Seismicity, normal faulting, and the geomorphological development of the Gulf of Corinth (Greece): the Corinth earthquakes of February and March 1981. *Earth planet. Sci. Lett.* **57**, 377-397.
- Jarpe, S.P. and P.W. Kasameyer (1996). Validation of a Procedure for Calculating Broadband Strong Motion Time Histories from Empirical Green's Functions. *Bul. Seis. Soc. Am.* **86**, 1116-1129.
- Joyner, W. B. and D. M. Boore (1986). On simulating large earthquakes by Green's-function addition of smaller earthquakes, *Earthquake Source Mechanics*, Geophysical Monograph No. 37, Maurice Ewing, Ed., **8**, 269–274.
- Kalogeras, Ioannis S. and George N. Stavrakakis (1996) Strong motion records and their analysis in the Geodynamics Institute of the National Observatory of Athens.
- Kennett, B. L. N. (1983) *Seismic Wave Propagation in Stratified Media*, Cambridge University Press, Cambridge.
- Kostrov, B.V. and S. Das (1988) Principles of earthquake source mechanics, in *Cambridge Monographs on Mechanics and Applied Mathematics*, Cambridge University Press, Cambridge.
- McCallen, D.B. and L.J. Hutchings (1996) Ground motion estimation and nonlinear seismic analysis. Lawrence Livermore National Laboratory, Livermore, CA, UCRL-JC-121667. proceedings: 12th Conference on Analysis and Computation of the American Society of Civil Engineers, Chicago.
- Munguia, L. and J. Brune (1984). Simulation of strong ground motion for earthquakes in the Mexicali-Imperial Valley region, *Geophys. J. Royal Astr. Soc.* **79**, 747–771.
- Papageorgiou, A.S. and K. Aki (1983). A specific Barrier model for the Quantitative description of inhomogeneous faulting and the prediction of strong ground motion. I. Description of the model. *Bul. Seis. Soc. Am.* **73**, 693–722.
- Rice, J.R. and A.L. Ruina (1983) Stability of steady friction slipping. *J. Appl. Mech.*, **105**, 343-349.
- Stavrakakis, G.N., J. Drakopoulos and K. Makropoulos (1982) A rupture model for the Corinth earthquake sequence of 1981. *Earth Planet. Lett.*, **57**, 377-397.
- Tselentis, Gerasimos-Akis and Kostas C. Makropoulos (1986) Rates of Crustal Deformation in the Gulf of Corinth (Central Greece) as determined from seismicity. *Tectonophy.*, **124**, 55-66.
- Wald, D.J., D.V. Helmberger and S.H. Hartzell (1990) Rupture process of the 1987 Superstition Hills Earthquake from inversion of Strong-Motion Data. *Bul. Seis. Soc. Am.* **80**, 1079–1098.
- Wald, David J., Donald V. Helmberger, and Thomas H. Heaton (1991) Rupture Model of the 1989 Loma Prieta Earthquake from Inversion of Strong-Motion and Broadband Teleseismic Data. *Bul. Seis. Soc. Am.* **81**, 1540–1572.
- Wald, D. J., T. H. Heaton, and K.W. Hudnut (1995) The Slip History of the 1994 Northridge, California Earthquake Determined from Strong -Motion, Teleseismic, GPS, and Leveling Data. preprint, *Bul. Seism. Soc. Am.* **81** (1).
- Wennerberg, L. (1990). Stochastic summation of empirical Green's functions, *Bul. Seis. Soc. Am.* **80**, 1418–1432.
- Wu, F. T. (1978). Prediction of Strong Ground Motion using Small Earthquakes, *Proc. 2nd International Microzonation Conference 2*, 701–704.
- Wu, Francis T., Ruey-Juin Rau, and David Salzberg (1996) Taiwan Orogeny: Thin-Skinned or Lithospheric Collision? preprint, *Tectonophysics*.
- Scholz, C.H. (1990) *The mechanics of Earthquake Faulting*, Cambridge University Press, Cambridge, 439p.
- Tumarkin, A.G., R.J. Archuleta, and R. Madariaga (1994) Basic scaling relations for composite models, *Bull. Seism. Soc. Am.* **84**, no 4.
- Vita-Finzi, C. and G.C. King (1985) The seismicity, geomorphology and structural evolution of the Corinth Area of Greece. *Phil. Trans. R. Soc. Lond. A* **314**, 379-407.